# FEM-BEM modeling of nonlinear magnetoelectric effects in heterogeneous composite structures

A. Urdaneta-Calzadilla, N. Galopin, I. Niyonzima, Olivier Chadebec, G. Meunier, B. Bannwarth

# FEM-BEM modeling of nonlinear magnetoelectric effects in heterogeneous composite structures

A. Urdaneta-Calzadilla [1], N. Galopin [1], I. Niyonzima [1] O. Chadebec [1], G. Meunier [1], B. Bannwarth [1]

[1] Univ. Grenoble Alpes, CNRS, Grenoble INP, G2Elab, F-38000 Grenoble, France

**This paper proposes a multiphysics multi-method model for 3D nonlinear magnetoelectric effects in heterogeneous composite structures made of the association of piezoelectric and magnetostrictive materials. Through the coupling of the Finite Element Method with the Boundary Element Method, only the active material is explicitly considered, and thus a single mesh is used for the resolution of all the physics. A mixed formulation combining the vector potential in the volume and a scalar potential in the free space is used to model magnetic phenomena. Non-linear constitutive laws for the magnetostrictive phase are derived from partial derivatives of a scalar invariant's formulation of the Helmholtz free energy, while linear relations are used to describe piezoelectric behavior. The coupled problem is solved by iteratively solving single-physics problems, and the full algorithm is used to model a rotating coilless ME device which can operate as an energy harvester or as an actuator.**

***Index Terms*—Boundary element methods, Finite element analysis, Magnetoelectric effects, Rotating coilless ME device.**

## I. Introduction

ELECTROMAGNETIC interaction can be achieved by magnetoelectric (ME) composites. These materials are based on mechanical exchanges through the combination of piezoelectric and magnetostrictive materials which have, respectively, strong electro-mechanical and magneto-mechanical couplings [1]. Numerical modeling of these phenomena is usually performed through the Finite Element Method (FEM) [2], [3]. Nevertheless, to correctly account for the decay of magnetic fields at infinity, the FEM needs a big enough free space domain to be explicitly considered and meshed. As a result, a large number of degrees of freedom being located outside the active material, notably with regard to the quantity of active materials and their distance from the sources. This can be avoided by setting up a coupling between the Boundary Element Method (BEM) and the FEM for the magnetic part, and the FEM for the electric and mechanical parts. The coupling between FEM and BEM has proved to be a powerful tool for reducing computational time and allocated memory for solving multi-physics problems, and enabling the use of a single mesh for all the problems concerned (see e.g., [4] by the authors). It should be noted, however, that this previous work was limited to a linearized approach to magneto-mechanical effects, which severely limited the validity of the model.

Contrary to piezoelectricity which in most situations can be accurately described by linear relations, magneto-mechanical behavior is strongly nonlinear. Many approaches have been taken to consider this non-linearity. In this paper, we implemented the description of magneto-mechanical behavior in terms of a scalar invariant's formulation of the Helmholtz free energy [5]. This approach has already been used in a purely FEM context. The main contribution of this article is to extend it to FEM-BEM coupling. We will see that this extension leads to numerical difficulties, which have been resolved by using an adaptive iterative approach of nonlinear single-physics problems.

In the rest of the paper, we present the material laws and the formulations used in the model. Then the model is used to simulate a rotating coilless ME device under the influence of a permanent magnet. This device can operate as an energy harvester or as an actuator. In particular, in actuator mode, the calculation of magnetic forces is discussed using two approaches: the magnetic charge method and the Laplace force.

## II. Constitutive laws

The considered behavioral law for the piezoelectric phase is given by the two linear coupled relationships (1),

$$\begin{aligned} \boldsymbol{T}(\boldsymbol{S},\boldsymbol{E}) &= \boldsymbol{C}^{\boldsymbol{E}} : \boldsymbol{S} - {}^{t}\boldsymbol{e}\cdot\boldsymbol{E}, \\ \boldsymbol{D}(\boldsymbol{S},\boldsymbol{E}) &= \boldsymbol{e} : \boldsymbol{S} + \boldsymbol{\varepsilon}^{\boldsymbol{S}}\cdot\boldsymbol{E}, \end{aligned} \tag{1}$$

with $\boldsymbol{D}$ the electric displacement field, $\boldsymbol{E}$ the electric field, $\boldsymbol{T}$ the Cauchy stress tensor, $\boldsymbol{S}$ the linear strain tensor, $\boldsymbol{C}^{E}$ the elasticity tensor at constant electric field, $\boldsymbol{e}$ the piezoelectric tensor and $\boldsymbol{\varepsilon}^{S}$ the permittivity tensor at constant strain." $\cdot$ ", " : " and ${}^{t}\bullet$ denote respectively the dot product, the double dot product and the transpose operator.

Inside the magnetostrictive phase, the Helmholtz free energy $\psi$ can be expressed in the case of isotropic materials as a polynomial expression on its invariants $I_i$ [5]:

$$\psi = \frac{1}{2}\lambda I_1^2 + \mu I_2 + \sum_{i=1}^{n_\alpha}\alpha_i I_4^i + \sum_{i=1}^{n_\beta}\beta_i I_5^i + \sum_{i=1}^{n_\gamma}\gamma_i I_6^i, \tag{2}$$

where:

$$\begin{aligned} I_1 = tr(\boldsymbol{S}),\ I_2 = tr(\boldsymbol{S}^2), I_4 = \boldsymbol{B}\cdot\boldsymbol{B} \\ I_5 = \boldsymbol{B}\cdot\tilde{\boldsymbol{S}}\cdot\boldsymbol{B},\ I_6 = \boldsymbol{B}\cdot\tilde{\boldsymbol{S}}^2\cdot\boldsymbol{B}, \end{aligned} \tag{3}$$

with $\boldsymbol{B}$ the magnetic induction, $\boldsymbol{H}$ the magnetic field, $\tilde{S}$ the deviatoric part of the strain tensor, $\lambda$ and $\mu$ the Lamé coefficients of the material, $\alpha_i$, $\beta_i$ and $\gamma_i$ a finite set of scalar coefficients. The magnetic and mechanical coupled nonlinear behavioral laws can then be obtained by the analytical differentiation of the energy $\psi$:

$$\boldsymbol{T}(\boldsymbol{B},\boldsymbol{S}) = \frac{\partial\psi}{\partial\boldsymbol{S}}, \quad \boldsymbol{H}(\boldsymbol{B},\boldsymbol{S}) = \frac{\partial\psi}{\partial\boldsymbol{B}}. \tag{4}$$

The behavior of ME composite structures is then obtained through the combination of (1) and (4).

## III. Formulations and Resolution Method

The electrical and mechanical problems are limited to the active domain $\Omega_m$ [4]. Indeed, because of the high permittivity of piezoelectric materials and since the electrodes are in direct contact with the piezoelectric materials, the electric displacement field is canalyzed inside the materials. Therefore, restricting the domains to $\Omega_m$ is a reasonable approximation. Considering static behaviour, from Maxwell-Gauss relation, (1) and appropriate boundary conditions, the electric weak form in terms of electric scalar potential ($\boldsymbol{E} = -\nabla\varphi$) reads, find $\varphi$ such that:

$$\int_{\Omega_m} \nabla\delta\varphi \cdot \boldsymbol{D}(\boldsymbol{S}, \boldsymbol{E})\ d\Omega = 0 \quad \forall\delta\varphi. \tag{5}$$

with $\delta\varphi$ an appropriate virtual electric scalar potential field. From (1), (4) and the balance of linear momentum, the mechanical weak form in terms of mechanical displacement $\boldsymbol{u}$ reads, find $\boldsymbol{u}$ such that:

$$\int_{\Omega_m} \nabla^S\boldsymbol{\delta u} : \boldsymbol{T}(\boldsymbol{S}, \boldsymbol{E}, \boldsymbol{B})\ d\Omega = 0 \quad \forall\delta\boldsymbol{u}, \tag{6}$$

where $\nabla^S\boldsymbol{u} = \frac{1}{2}(\nabla\boldsymbol{u} + (\nabla\boldsymbol{u})^t)$ and $\delta\boldsymbol{u}$ an appropriate virtual mechanical displacement vector field. Both (5) and (6) are discretized using first order FEM and nodal shape functions. Similarly to [6], the weak form of the magnetic problem is obtained by testing Maxwell-Ampere's equation, keeping the boundary term. It reads, find $(\boldsymbol{a}, \phi_{red})$ such that:

$$\begin{aligned}\int_{\Omega_m} \nabla\times\delta\boldsymbol{a}\cdot\boldsymbol{H}(\boldsymbol{B},\boldsymbol{S})\ d\Omega + \int_{\partial\Omega_m} \nabla\times\delta\boldsymbol{a}\cdot n\ \phi_{red}\ d\partial\Omega \\ = \int_{\partial\Omega_m} (\delta\boldsymbol{a}\times n)\cdot\boldsymbol{H_0}\ d\partial\Omega \quad \forall\delta\boldsymbol{a},\end{aligned} \tag{7}$$

with $\boldsymbol{a}$ the magnetic vector potential ($\boldsymbol{B} = \nabla\times\boldsymbol{a}$), $\delta\boldsymbol{a}$ an appropriate virtual magnetic vector potential field , $\phi_{red}$ the magnetic reduced scalar potential, $\boldsymbol{H_0}$ the magnetic field created by the currents external to the domain calculated by the Biot-Savart law and $\boldsymbol{n}$ the outwards normal vector to $\partial\Omega_m$. The previous equation is discretized using edge elements for $\boldsymbol{a}$ and 0-order surface elements for $\phi_{red}$. To describe the behavior of the magnetic field at the boundary, we add to this system of equations a discretized form of Green's third identity applied to the reduced magnetic scalar potential $\phi_{red}$. Indeed, at the boundary of the free space domain $\Omega_0$, $\Delta\phi_{red} = 0$. Green's third identity applied to $\phi_{red}$ reads,

$$\begin{aligned}\frac{1}{2}\phi_{red} + \int_{\partial\Omega_m} G\frac{\boldsymbol{B}\cdot\boldsymbol{n}}{\mu_0}\ d\partial\Omega - \int_{\partial\Omega_m}\phi_{red}\frac{\partial G}{\partial n}\ d\partial\Omega \\ = \int_{\partial\Omega_m} G\ \boldsymbol{H}_0\cdot\boldsymbol{n}\ d\partial\Omega.\end{aligned} \tag{8}$$

with $G$ the Green's kernel. Equation (8) is then projected onto surface test functions constant by surface cell element, $\phi_{red}$ is discretized with the same 0th-order surface shape functions. Magnetic induction leakage, $B_n$, is linked to the circulation of the magnetic vector potential on the edge elements of the active domain boundary $\partial\Omega_m$, via an incidence matrix resulting from the local application of Stokes' theorem to the edges of a facet element. The outside and inside magnetic problems are then coupled via the continuity of $\boldsymbol{B}\cdot\boldsymbol{n}$ and $\phi_{red}$ across $\partial\Omega_m$. BEM matrices are full and are compressed using the Fast Multipole Method (FMM) [7] to reduce storage space up to 80

## IV. Solving the Discretized ME Problem

The presence of both full BEM matrices and sparse FEM matrices makes the resolution of the fully coupled discrete problem difficult. This is associated with poor conditioning of the global system which results from the difference in the scale of the physics involved (MPa vs $\mathrm{Fm}^{-1}$ vs $\mathrm{mH}^{-1}$). A coupled multiphysics solution can be obtained from the iterative resolution of single-physics problems [4].

An adaptive algorithm for the choice of the problem to be solved, which solves in priority the problem with the worst convergence, is used. MUMPS direct solver is used to solve the discretized electric equation while the Newton-Raphson method is used to solve the nonlinear mechanical and magnetic problems. They are based on a preconditioned BiCGSTAB solver for the discretized mechanical equation and a preconditioned GMRES for the discretized magnetic problem. An incomplete LU is used for the FEM block of the magnetic problem, while a Jacobi preconditioner is used for the diagonal BEM block.

## V. Validation of the Magneto-Mechanical Formulation

The magneto-mechanical formulation was validated with respect to the analytical solution of a Galfenol sphere under a uniform source field and uniaxial stress. It involved solving for $(\boldsymbol{B}, \boldsymbol{S})$ in $H = \frac{3\ H_0}{\mu_r+2}$, with $\mu_r = B/\mu_0 H$, both supposed scalar and uniform because of the considered spherical geometry, with $\boldsymbol{H_0}$ oriented along the (z) direction, together with solving for $(\boldsymbol{B}, \boldsymbol{S})$ in $T_{zz} = T_0$. Figure 1 shows the $L^2$ error of the formulation compared to the analytical solution [4]. They show the h-convergence of the formulation for $H_0$ = 200 $\mathrm{kAm}^{-1}$ and $T_0$ = 10 MPa.

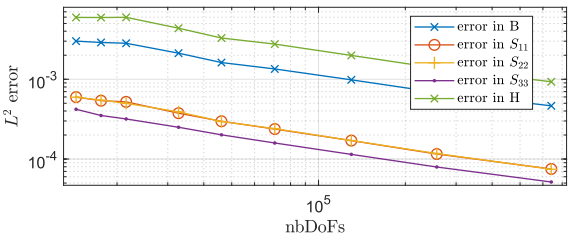


Fig. 1. $L^2$ error of the magneto-mechanical solutions compared to the analytical solutions vs the number of total DoFs of the magneto-mechanical problem.

## VI. Rotating Coilless ME Device

The directions of easy magnetization in magnetostrictive materials are dependent on both the magnetic state and the state of stress. Depending on how these easy magnetization directions are controled in the magnetostrictive layer, two modes of operation of the ME composite are possible.

To illustrate these behaviors, we consider the structure presented in Figure 2 which constitutes a rotating coilless ME

device. The device consists of a layer of a piezoelectric material, PZT-5A [8], on which four electrodes are arranged, and a layer of a disk-shaped magnetostrictive material consisting of Galfenol. This composite is subjected to the magnetic field of a NdFeB permanent magnet, with a remanent field of 1.13 T, free to rotate and spatially referenced by the angle $\hat{\theta}$ (Fig. 2) corresponding to the direction of its polarization. An Amperian description is considered for the permanent magnet.

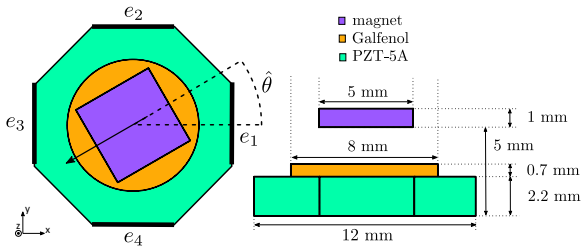


Fig. 2. Test device, the arrow corresponds to the direction of the remanent field in the magnet, $e_1$, $e_2$ , $e_3$ and $e_4$ refer to electrodes. Coefficients for Galfenol at 0 MPa has been obtained by a numerical fitting of experimental data from [5] : $\alpha_1 = 1514.2433$, $\alpha_3 = 91.2778$, $\alpha_5 = 64.8796$, $\alpha_6 = -113.9582$, $\alpha_7 = 44.2302$, $\alpha_{10} = -1.3699$, $\alpha_{11} = 0.2859$, $\beta_1 = -6.9705 \cdot 10^6$, $\gamma_1 = 1.1280 \cdot 10^{10}$, $\gamma_2 = -6.9770 \cdot 10^5$, $\alpha_2 = \alpha_4 = \alpha_8 = \alpha_9 = 0$.

The poling pattern of the piezoelectric phase is considered fixed, and the piezoelectric material poled by the application of electric potentials to a specific configuration of the electrodes: 1 kV on $e_3$ and $e_4$ and 0 V on $e_1$ and $e_2$. This results in a poling pattern mainly along the $\hat{\theta} = \pi/4$ (Fig. 2). Numerically, this poling pattern was obtained by the rotation of the piezoelectric tensors $\boldsymbol{C}$, $\boldsymbol{e}$ and $\boldsymbol{\varepsilon}$ in the direction of the electric field obtained by an electrostatic resolution.

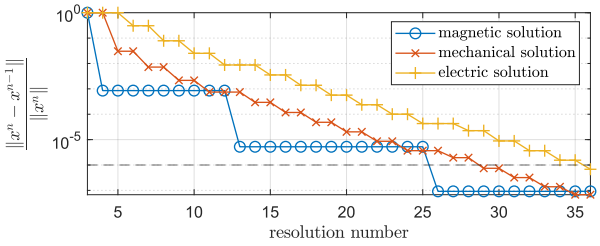


Fig. 3. Convergence of the single-physics solutions in generator mode within the multi-physics solver for the ME generator at $\hat{\theta}$ = 0 rad.

### A. Discrete system

The geometry was discretized into 27,055 nodes, 54,944 tetrahedral elements and 33,992 triangular elements for the surface of the magnet. This translates into 79,573 magnetic DoFs, 34,443 mechanical DoFs and 11,011 electrical DoFs. For every resolution of the mechanical problem, it takes around 21 iterations of the mechanical Newton-Raphson for the residue to converge within a relative tolerance of $10^{-7}$. The magnetic Newton-Raphson converges in 2 iterations to the same tolerance. The number of resolutions needed to reach a convergence of all solutions to relative $10^{-6}$ in generator and actuator mode are presented in Table I and the convergence of the three single-physics solutions presented in Figure 3.

The total integration time of BEM and linear FEM matrices was of 36 s and the resolution time of each simulation of ME

TABLE I
NUMBER OF SINGLE-PHYSICS RESOLUTIONS NEEDED FOR CONVERGENCE OF THE MULTIPHYSICS PROBLEM WITH TOLERANCE INFERIOR TO $10^{-6}$

| Problem | Generator | Actuator (1 kV) |
|---|---|---|
| Magnetic | 4 | 4 |
| Electric | 16 | 15 |
| Mechanical | 16 | 15 |

device took around 2 h on a computer equipped with Intel© Xeon© Gold 6240R CPU @ 2.4 GHz, 256 Gb of RAM.

### B. Actuator Mode

In actuator mode, it is the stress field in the magnetostrictive layer, generated by the piezoelectric layer, which controls the directional magnetic anisotropy. By applying a positive electric voltage $V_{in}$ between the electrodes $e_1$-$e_2$ and electrodes $e_3$-$e_4$, the piezoelectric layer mainly produces tension in the Galfenol layer. This induces a change in the direction of magnetization. As a result, the magnetic interaction between the Galfenol and the magnet produces a volumic torque, tending to align the polarization of the magnet with the easy axis of the Galfenol disk.

The torque $\Gamma$ was computed by two methods. In the Galfenol layer ($\Omega_{mm}$), the classical magnetic charge method [9] as been used:

$$\boldsymbol{\Gamma} = \int_{\Omega_{mm}} \boldsymbol{r} \times (\nabla \cdot \boldsymbol{M})\, \boldsymbol{H}_{magnet}\, d\Omega, \tag{9}$$

with $\boldsymbol{M}$ the magnetization of the Galfenol layer and $H_{magnet}$ the magnetic source field created by the magnet. For the computation of the torque acting on the permanent magnet, a most efficient way is to consider equivalent current for the magnet magnetization. The torque is then simply computing considering the Laplace field current interaction.

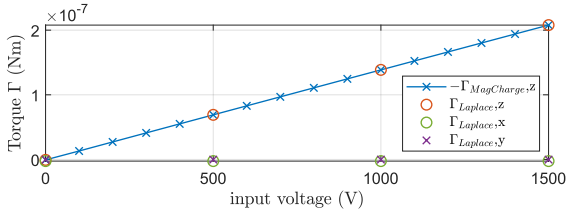


Fig. 4. Global torque $\Gamma$ between the Galfenol disk and the magnet vs the voltage applied to the piezoelectric layer. It is computed as a Laplace force in the magnet, and, its (z) component is compared to the torque computed by the magnetic charge method in the Galfenol layer.

Figure 4 shows the global torque as a function of the input voltage. To study the dependence of the angle $\hat{\theta}$ onto the torque, the rotation of the magnet on a complete turn is discretized into 32 angles, and the magnetic force computed with the two previous methods for an input voltage $V_{in}$ = 1 kV. Each computation of the torque by the magnetic charge method takes around 22 s while the computation of the Laplace force takes around 3 h, for 64 Gauss point at each of the magnets triangular surface elements.

In Figure 5 we see the mechanical torque as a function of the angle $\hat{\theta}$. We see that for angles $\pi/4$, $3\pi/4$, $5\pi/4$ and $7\pi/4$ rad, the torque is equal to zero. This is because at these angles the mechanical anisotropy induced by the mechanical

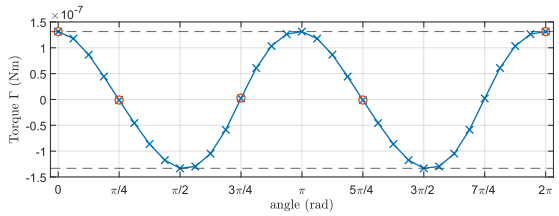


Fig. 5. Torque $\Gamma$ vs rotation angle $\hat{\theta}$. Cross markers correspond to the z-component of the torque in the Galfenol layer $(-\Gamma, z)$, circle markers correspond to the z-component of the torque in the magnet, for 33 angles $\hat{\theta}$ describing the full rotation of the magnet.

loading of the Galfenol phase is in the same direction as the magnetization. There is therefore no global shifting in the direction of magnetization in the Galfenol phase and, therefore, the torque in the (z) direction is equal to zero. Conversely, angles 0, $\pi/2$, $\pi$ and $3\pi/2$ rad correspond to maxima of the torque. Given the poling pattern of the electrodes, which results in a poling and mechanical traction along the $\pi/4$ rad direction, the anisotropy of the magnetization in the Galfenol layer is maximal for $\hat{\theta}$ equal to directions multiple of $\pi/2$ rad, i.e, $\pi/4$ rad relative to the $\pi/4$ rad main poling direction.

### C. Generator mode

In the generator mode, it is the rotation of the magnet that controls the direction of the magnetization in the magnetostrictive layer and, thus, the deformations of the ME composite. This leads to the appearance of a electric potential difference between the electrodes, which is dependent on the angle of rotation $\hat{\theta}$ (Fig. 2). The rotation of the magnet during a complet revolution is again discretized into 32 angles, and the previous poling pattern is considered. The electrodes are configured as follows: reference potential for electrodes $e_1$ and $e_2$, floating potential for electrodes $e_3$ and $e_4$.

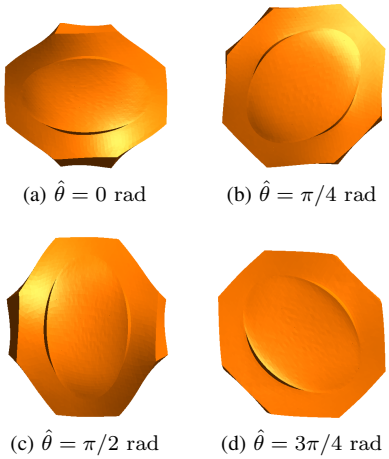

(a) $\hat{\theta} = 0$ rad (b) $\hat{\theta} = \pi/4$ rad

(c) $\hat{\theta} = \pi/2$ rad (d) $\hat{\theta} = 3\pi/4$ rad

Fig. 6. Amplified displacements ($\times 10^5$) of the ME composite for angles $\hat{\theta} = 0, \pi/4, \pi/2$ & $3\pi/4$ rad, top view

Figures 6a-6d show the amplified displacements ($\times 10^5$) of the device. They illustrate its mechanical response to the magnetic excitation. They show that the deformation of the device occurs mainly along the angle $\hat{\theta}$ even if some slight anisotropies in the mechanical response are visible for $\hat{\theta} =$ 0 & $\pi/2$ rad. These anisotropies in the mechanical response can be explained by the anisotropic mechanical properties of poled PZT-5A.

In Figure 7 is presented the output voltage of the ME composite vs the angle $\hat{\theta}$ between the magnet and the structure. We observe a sinusoidal output voltage with two periods per rotation of the magnet. This is because the magnetostrictive strains depend only on the direction of the applied field and not on its sense.

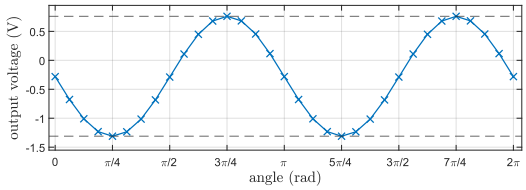


Fig. 7. Potential difference between the reference electrodes, $e_1$ and $e_2$, and the floating potential electrodes, $e_3$ and $e_4$, vs the angle $\hat{\theta}$ between the magnet and the ME composite.

## VII. Conclusion

In this paper we present a FEM-BEM coupling strategy used for modeling nonlinear ME effects in composite structures. While using a formulation similar to [6], nonlinear coupled constitutive laws are used for the magnetostrictive phase. We adopted an invariant description of the Helmholtz free energy to derive the nonlinear expressions of the Cauchy stress tensor and the magnetic field in order to model the magneto-mechanical behavior of Galfenol. We solved for the complete multiphysics problem by solving iteratively the three derived single-physics problems. The full algorithm was successfully tested on the modeling of a rotating coilless ME device in generator and actuator mode. In particular, two methods for computing the mechanical torque were presented and gave very close results. However, the magnetic charge method proved to be much faster at computing magnetic forces.

## References


[1] W. Eerenstein, N. D. Mathur, J. F. Scott, "Multiferroic and magnetoelectric materials," *Nature*, vol. 442, pp. 759–765, 2006.

[2] T. T. Nguyen, F. Bouillault, L. Daniel, X. Mininger, "Finite element modeling of magnetic field sensors based on nonlinear magnetoelectric effect," *J. Appl. Phys.*, vol. 109, no. 8, Apr. 2011, Art. no. 084904.

[3] H. Talleb, Z. Ren, "Finite element modeling of magnetoelectric laminate composites in considering nonlinear and load effects for energy harvesting," *J. Alloys Comp.*, vol. 615, pp. 65-74, 2014.

[4] A. Urdaneta-Calzadilla, N. Galopin, I. Niyonzima, O. Chadebec, B. Bannwarth, G. Meunier, "A FEM-BEM coupling strategy for the modeling of magnetoelectric effects in composite structures," *Eng. Anal. Bound. Elem.*, vol. 151, pp. 41-55, 2023.

[5] U. Ahmed, U. Aydin, L. Daniel, P. Rasilo, "3-D Magneto-Mechanical Finite Element Analysis of Galfenol-Based Energy Harvester Using an Equivalent Stress Model," *IEEE Trans. Magn.*, vol. 57, no. 2, pp. 1-5, Feb. 2021, Art no. 7400405.

[6] A. Urdaneta-Calzadilla, O. Chadebec, N. Galopin, I. Niyonzima, G. Meunier and B. Bannwarth, "Modeling of Magnetoelectric Effects in Composite Structures by FEM–BEM Coupling," *IEEE Trans. Magn.*, vol. 59, no. 5, pp. 1-4, May 2023, Art no. 7000604.

[7] L. Greengard, V. Rokhlin, "A fast algorithm for particle simulations," *J. Comput. Phys*, vol. 73, no. 2, pp. 325–348, 1987.

[8] Jemai, Ajmi, et al. "Advanced Parametric Analysis of piezoelectric actuators with Interdigitated Electrodes having Various Cross-Sections," in *Proc. Design and Modeling of Mechanical Systems - II. Lecture Notes in Mechanical Engineering*. Springer, Cham, 2015.

[9] E. Durand, *Magnétostatique*. Paris, France, Masson et Cie, 1968.